Monthly Notices of the ROYAL ASTRONOMICAL SOCIETY

MNRAS **532,** 2905–2919 (2024) https://doi.org/10.1093/mnras/stae1564
Advance Access publication 2024 June 27

Metal factories in the early Universe

Stephen Eales,[1]★ Haley Gomez [1], Loretta Dunne,[1] Simon Dye [2] and Matthew W. L. Smith [1]

[1]*Cardiff Hub for Astrophysics Research and Technology, Cardiff University, The Parade, Cardiff CF24 3AA, UK*
[2]*School of Physics and Astronomy, University of Nottingham, University Park, Nottingham NG7 2RD, UK*

Accepted 2024 June 18. Received 2024 June 5; in original form 2023 November 23

ABSTRACT

We have estimated the mass of metals in the molecular gas in 13 dusty star-forming galaxies at $z \sim 4$ in which the gas, based on previous observations, lies in a cold rotating disc. We estimated the metal masses using either the submillimetre line or continuum emission from three tracers of the overall metal content – carbon atoms, carbon monoxide molecules, and dust grains – using the first simultaneous calibration of all three tracers. We obtain very similar mass estimates from the different tracers, which are similar to the entire metal content of a present-day massive early-type galaxy. We used the dynamical masses of these galaxies to estimate an upper limit on the mass of the molecular gas in each galaxy, allowing us to estimate a lower limit on the metal abundance of the gas, finding values for many of the galaxies well above the solar value. We show that the high metal masses and metal abundances are what is expected shortly after the formation of a galaxy for a top-heavy IMF. We suggest a scenario for galaxy evolution in which massive galaxies reach a high metal abundance during their formation phase, which is then gradually reduced by dry mergers with lower mass galaxies. We show that the metals in the outflows from high-redshift dusty star-forming galaxies can quantitatively explain the long-standing puzzle that such a large fraction of the metals in galaxy clusters ($\simeq$0.75) is in the intracluster gas rather than in the galaxies themselves.

Key words: galaxies: abundances – galaxies: evolution – galaxies: formation – galaxies: high-redshift – galaxies: ISM – submillimetre: galaxies.

1 INTRODUCTION

One of the most distinctive properties of the galaxy population today is the strong relationship between metal abundance and stellar mass, with metal abundance increasing with stellar mass and reaching a value of about twice the solar value at the highest masses (Gallazzi et al. 2005). Prior to the launch of the JWST, there was evidence that this relationship already existed for galaxies at $z \sim 3-5$, although with the metal abundances a factor of $\simeq$4 lower than for galaxies with the same stellar mass in the Universe today (Cullen et al. 2019). Recent JWST observations have now shown this relationship was already in place at $z \sim 10$, with the metal abundances lower by a factor of $4-10$ at the same stellar mass from the relationship today (Fujimoto et al. 2023; Heintz et al. 2023; Langeroodi et al. 2023; Curti et al. 2024).

Lower metal abundances for galaxies at high redshifts are, of course, not really surprising because there has been less time than for metals to have been made in stars and ejected into the ISM. Nevertheless, there are signs in the Universe today that there must have been a period of rapid metal production early in the history of the Universe. The best evidence comes from rich clusters of galaxies, in which the strong gravitational fields ensure that no metals should have been lost from the cluster. In nearby rich clusters, roughly 75 per cent of the metals are in the intracluster gas rather than in the galaxies (Portinari et al. 2004; Loewenstein 2013; Renzini & Andreon 2014; Mernier & Biffi 2022). Clusters today are dominated by elliptical and lenticular galaxies – early-type galaxies – in which the current rate of star formation, and therefore metal production, is low. The best estimates, based on the spectra of these galaxies, suggest that most of their stars were formed during the first two billion years after the big bang during a burst of star formation lasting only $\simeq 5 \times 10^8$ years (Thomas et al. 2010). It therefore seems likely that most of the metals that are in the intracluster gas today were formed during this early period of star formation and then ejected from the galaxies, although models based on this assumption have so far failed to reproduce the mass of metals in the intracluster gas by a factor of between 2 and 10 (Loewenstein 2013; Renzini & Andreon 2014).

The estimated star-formation rates of these galaxies during this early period of star formation lie in the range 100–1000 $M_\odot$ year^{-1}. Twenty-five years after they were discovered, the galaxies found in the first submillimetre surveys (Smail, Ivison & Blain 1997; Barger et al. 1998; Hughes et al. 1998; Eales et al. 1999) are still the only galaxies in the correct redshift range and with the necessary star-formation rates to be the ancestors of the massive early-type galaxies in present-day clusters (Hughes et al. 1998; Lilly et al. 1999). The wide-field submillimetre surveys with the *Herschel Space Observatory* and the South Pole Telescope (SPT) have discovered many examples of these dusty star-forming galaxies (henceforth DSFGs) with a star-formation rate > 1000 $M_\odot$ year^{-1} (Bakx et al. 2018; Reuter et al. 2020).

★ E-mail: EalesSA@cardiff.ac.uk

The DSFGs must contain a large mass of dust, which is mostly composed of metals, and they are therefore an exception to the metal-poor high-redshift Universe revealed by the early JWST observations. The dust, however, makes it challenging to use standard optical techniques to measure their metal abundance, with estimates of the visual extinction often having extreme values (e.g. $A_V > 450$ - Harrington et al. (2021)). On top of this problem, there is the additional problem that many of the brightest DSFGs are gravitationally lensed, which means there is a bright galaxy sitting in front of the DSFG, contaminating its optical emission.

In this paper, we have developed an alternative way of estimating the mass of metals and the metal abundance in these galaxies. A widely used technique for estimating the mass of the molecular gas in a galaxy is to use the luminosity of a tracer of the gas to estimate its mass. Carbon monoxide molecules (Bolatto, Wolfire & Leroy 2013; Tacconi, Genzel & Sternberg 2020), carbon atoms (Papadopoulos & Greve 2004), and dust grains (Eales et al. 2012; Scoville et al. 2016, 2017; Tacconi et al. 2020) have all been tried.

Whichever of the tracers is used, the calibration of this method is ultimately based almost always on observations of the ISM in the Galaxy, which suggests two obvious objections. The first is that an implicit assumption of the method is that the conditions in the galaxy of interest – the density, temperature, and structure of its molecular gas, the physical and chemical properties of its dust grains – are the same as in the Galaxy. The second objection, since all the tracers are made of metals, is that an implicit assumption of the method is that the metal abundance is the same as in the Galaxy. Given the evolution seen in the relationship between metal abundance and stellar mass (see above), this assumption seems particularly dubious if the galaxy of interest is at high redshift (Scoville et al. 2016, 2017; Tacconi et al. 2020).

The second objection can be avoided if the method, as we do here, is used to estimate the mass of the metals rather than the mass of the molecular gas, since it then does not rely on any assumption about the metal abundance. Dunne et al. (2022) have made the first attempt to calibrate the tracer method which treats all tracers equally rather than relying on one as a gold standard to calibrate the others (Appendix A). We have used these new calibration factors to estimate the mass of metals in the molecular gas for a sample of DSFGs at $z \sim 4$. Although our method avoids the assumption of a universal metal abundance, it still relies on the assumption that the critical properties of the ISM on which the emission from the tracers depend are the same as in the Galactic ISM.

This method is a way of estimating the total mass of metals but not the metal abundance, which *does* require knowledge of the mass of the molecular gas. However, we can estimate an upper limit on the mass of the gas from an estimate of the dynamical mass of the galaxy. A large proportion of the extreme DSFGs discovered with *Herschel* and the South Pole Telescope are magnified by gravitational lenses, which has made it possible to investigate the motion of the gas with resolution as high as 50 pc (Dye et al. 2015). Observations of the gas kinematics have revealed that the gas in many of these galaxies is distributed in a cold rotating disc (Hodge et al. 2012; Dye et al. 2015; Neeleman et al. 2020; Rizzo et al. 2020; Fraternali et al. 2021; Lelli et al. 2021; Rizzo et al. 2021; Dye et al. 2022), which makes it possible to estimate the mass of the galaxy from the circular velocity of the gas. By estimating the dynamical mass of each galaxy, we have estimated an upper limit on the mass of the molecular gas, which has allowed us to estimate a lower limit on the metal abundance.

The arrangement of the paper is as follows. Section 2 describes our sample of galaxies. In Section 3 we describe our method for estimating the mass of metals and the application of this method to our sample. In Section 4, we use the dynamical masses of the galaxies to estimate an upper limit on the mass of the molecular gas in each galaxy and thus a lower limit on the galaxy's metal abundance. In this section, we also propose a solution to the well-known paradox that the estimate of the mass of the molecular gas in a high-redshift galaxy is often greater than the estimate of its dynamical mass. In Section 5, we use chemical evolution models to interpret our results. In Section 6 we discuss our results and we list our conclusions in Section 7. We used the cosmological parameters given in Planck Collaboration et al. (2016).

Table 1. The sample.

Source	Redshift	Gravitational magnification	Reference
SPT0113-46	4.233	23.86 ± 0.51	1
ALESS073.1	4.76		2
SPT0345-47	4.296	7.95 ± 0.48	1
SPT0418-47	4.225	32.7 ± 2.66	1
SPT0441-46	4.48	12.73 ± 0.96	1
DLA0817g	4.26		3
SDP81	3.042	15.9 ± 0.7	4
AZTEC/C159	4.57		5,6
J1000+0234	4.54		5,6
GN20	4.05		7
ID141	4.24	5.5[a]	8
SPT2132-58	4.768	5.72 ± 0.54	1
SPT2146-55	4.567	6.65 ± 0.41	1

Note: References – 1: Reuter et al. (2020); 2: Lelli et al. (2021); 3: Neeleman et al. (2020); 4: Dye et al. (2015); 5: Jones et al. (2017); 6: Fraternali et al. (2021); 7: Hodge et al. (2012); 8: Dye et al. (2022). [a]Dye et al. (2022) do not give an error for the gravitational magnification factor, but all the gas and metal masses in this paper have been calculated from demagnified fluxes which have errors that incorporate the uncertainties in the lensing model. Also note that the ISM masses given by Dye et al. (2022) do not include a correction for the effect of the cosmic microwave background (Section 3.2).

2 THE SAMPLE

We selected a sample of 13 high-redshift galaxies for which there is evidence from the velocity profile (velocity versus radius) and from the high value of the ratio of rotational velocity to velocity dispersion (Section 4.1) that the gas in the galaxy lies in a cold rotating disc (Table 1).

All the galaxies also have observations that make it possible to estimate the mass of metals in the molecular gas, having at least one, and in most cases more than one, of the following observations: spectral line observations of C I 1–0; spectral line observations of either CO 1–0 or 2–1; continuum observations of dust.

The CO observations were mostly made with the Australia Telescope Compact Array (Aravena et al. 2016), which have a resolution of $\simeq 5$ arcsec. The C I observations were all made with the Atacama Millimeter Array (ALMA) (Bothwell et al. 2017; Dye et al. 2022). Apart from the high-resolution observations of ID141 (Dye et al. 2022), these have a resolution of $\simeq 5$ arcsec (Bothwell et al. 2017). Our main sources of dust observations were the compilation of multi-frequency global dust measurements for the SPT galaxies (Reuter et al. 2020) and our reanalysis of data in the ALMA archive (Section 3.1). In the case of the dust, there is almost always a high-resolution continuum image which makes it possible to be confident that the dust is within the region covered by the dynamical analysis e.g. Dye et al. (2015); Spilker et al. (2016); Dye et al. (2022).

Eight of the 13 galaxies are gravitationally lensed, and for each of these there is a lensing model with an estimate of the magnification and its uncertainty (Table 1). Twelve of the sample are at $z > 4$ when the Universe was less than 1.6 billion years old.

3 METAL MASSES

3.1 The method

Since molecular hydrogen does not itself emit spectral lines at the typical temperature of the molecular phase of the ISM, the standard method to estimate the mass of the molecular gas is from the luminosity (L) of some 'tracer'. The mass of the molecular gas is then given by the equation

$$M_{\rm mol} = \alpha L, \tag{1}$$

where α is a calibration factor. Carbon atoms (C I), CO, and dust grains have all been used as tracers. The calibration factor is almost always ultimately based on observations of the molecular gas in the Galaxy, from which it is possible to estimate the gas mass more directly, for example from gamma-ray observations or from the dynamical masses of molecular clouds (Bolatto et al. 2013; Tacconi et al. 2020). Over the last decade the application of this technique to high-redshift galaxies has led to the conclusion that as much as 90 per cent of the baryonic mass in a high-redshift galaxy is in the form of gas (Scoville et al. 2016, 2017; Tacconi et al. 2018).

As we noted above (Section 1), an obvious concern with this technique is that it relies on the assumption that the metal abundance is everywhere the same, which is especially dangerous when the galaxy is at high redshift. Nevertheless, although sometimes an attempt is made to correct the value of α for this effect using a measurement of the metal abundance in the galaxy (Tacconi et al. 2020), this measurement rarely has enough precision since the standard optical techniques for estimating metal abundance all themselves have large systematic uncertainties (Maiolino & Mannucci 2019). Therefore, for the want of anything better, the assumption that the calibration factors have the same values as in the Galaxy is the one that is often made.

In this paper, we try to avoid this problem by using observations of the tracers to estimate the mass of the metals rather than the mass of the molecular gas. We calculate the mass of metals in a galaxy from the luminosity of a tracer, L using the equation:

$$M = \alpha_{\rm MW}\, A_{\rm MW}\, L. \tag{2}$$

In this equation, $\alpha_{\rm MW}$ is the same calibration factor as in equation (1), to which we have added a subscript to show it is ultimately based on observations in the Galaxy (Milky Way), and $A_{\rm MW}$ is the metal abundance in the ISM in the Galaxy. We assume a metal abundance in the ISM in the Galaxy of 86.9, based on the latest estimates of the gas-to-dust ratio (167.2) and the fraction of the metals that is incorporated in the dust (0.52) (Roman-Duval et al. 2022).

This equation should still be correct even if the metal abundance in the galaxy that is being observed, $A_{\rm gal}$, is different from the value in the Galaxy. For the optically thin tracers, dust, and C I (Harrington et al. 2021; Papadopoulos, Dunne & Maddox 2022), the value of the calibration factor for the galaxy, $\alpha_{\rm gal}$, will be inversely proportional to the galaxy's metal abundance, and therefore $\alpha_{\rm gal} A_{\rm gal} = \alpha_{\rm MW} A_{\rm MW}$. This is not so obviously true for CO because the line emission is optically thick. Nevertheless, although the dependence of CO emission on metal abundance is still uncertain, the data does suggest a similar relationship between $\alpha_{\rm gal}$ and $A_{\rm gal}$ (fig. 9 of Bolatto et al. 2013). We emphasize that although we are now not making the assumption that the metal abundance is the same as in the Galaxy, we still need to make the assumption that the properties of the gas and dust on which the calibration factors depend are the same as in the Galaxy. For example, when using dust as the tracer we implicitly assume that the dust mass-opacity coefficient is the same as the Galactic value.

Table 2. Continuum measurements from observations in the ALMA archive.

Source	Frequency (GHz)	Flux density (μJy)	ALMA project code
ALESS 073.1	92.74	136 ± 22	2015.1.00040.S
J1000 + 0234	103.345	180 ± 31	2016.1.00171.S
SDP81	88.850	676 ± 98	2017.1.01694.S

We estimated the metal masses for the galaxies in the sample using observations of the following tracers: carbon atoms (C I), carbon monoxide molecules (CO), and dust grains, with calibration factors $\alpha_{\rm CI}$, $\alpha_{\rm CO}$, and $\alpha_{850\mu{\rm m}}$, respectively. We used the calibration factors from Dunne et al. (2022), which was the first attempt to calibrate all three calibration factors simultaneously. The values we assume are $1/\alpha_{850\mu{\rm m}} = 6.9 \times 10^{12}$ W Hz^{-1} M$_\odot^{-1}$ for the dust, $\alpha_{\rm CO} = 4.0$ M$_\odot$(K km s^{-1} pc^2)$^{-1}$ for the CO $J = 1 - 0$ line, and $\alpha_{\rm CI} = 17$ M$_\odot$(K km s^{-1} pc^2)$^{-1}$ for the CI $J = 1 - 0$ line. We assume the uncertainties in the calibration factors $\alpha_{850\mu{\rm m}}$, $\alpha_{\rm CO}$ and $\alpha_{\rm CI}$ are 31 per cent, 39 per cent and 19 per cent respectively, based on the values estimated in their paper.

We restricted ourselves to observations that are least likely to be affected by systematic uncertainties. We therefore used observations of atomic carbon in the C I $J = 1 - 0$ line but not in the C I $J = 2 - 1$ line because of the recent evidence of subthermal excitation, which leads to large uncertainties in the estimates of the mass of molecular gas from this line (Papadopoulos et al. 2022). We used observations of carbon monoxide in the $J = 1 - 0$ and $J = 2 - 1$ lines but not in the higher J lines because the ratio of the line flux for these lines to the line flux for the $J = 1 - 0$ line, on which the calibration is based, depends strongly on the temperature of the gas. We estimated a line flux for the $J = 1 - 0$ line from the line flux in the $J = 2 - 1$ line using the flux ratio CO2 $- 1/1 - 0 = 2.97 \pm 0.61$, which we derived from a study of carbon monoxide in a large sample of ultraluminous infrared galaxies (Papadopoulos et al. 2012).

We only used dust as a tracer if there was an observation close in rest-frame wavelength to 850 μm, the wavelength at which the dust method is calibrated (Dunne et al. 2022), which in practice mostly meant observations in ALMA Band 3. We found unpublished observations in the ALMA archive for three galaxies, and we measured new flux densities for these, which are given in Table 2. Where there were continuum observations at many wavelengths (Reuter et al. 2020) we fitted a modified blackbody ($F_\nu \propto B_\nu \nu^\beta$) to the flux densities at wavelengths $\geq 500\mu$m, using a single dust temperature and a dust emissivity index $\beta = 2$. The advantage of estimating the dust temperature from only long-wavelength flux measurements is that the estimate should be closer to the mass-weighted dust temperature; the inclusion of flux measurements on the short-wavelength side of the blackbody peak biases the estimate towards the luminosity-weighted dust temperature (Eales, Wynn-Williams & Duncan 1989). Our estimated dust temperatures for these galaxies are listed in Table 3 and they support the argument that the mass-weighted dust temperature, even for galaxies with very high star-formation rates, is$\simeq$ 25 K (Scoville et al. 2016). For these galaxies, we have estimated the rest-frame flux density at 850 μm

Table 3. The mass of metals.

Source	Metal masses with no CMB correction $(10^9\ M_\odot)$			Metal masses with CMB correction $(10^9\ M_\odot)$			T_d^a	Z	References
	CO	C I	Dust	CO	C I	Dust	(K)	$(Z_\odot)$	
SPT0113-46	0.79 ± 0.36	1.09 ± 0.30	0.58 ± 0.21	1.50 ± 0.69	1.70 ± 0.47	1.01 ± 0.37	19.8	0.99 ± 0.24	2,3,4
ALESS073.1	1.20 ± 0.60	...	2.42 ± 0.85	2.53 ± 1.26	...	3.93 ± 1.38		2.5 ± 0.9	1,5
SPT0345-47	2.58 ± 1.18	...	2.14 ± 0.79	4.95 ± 2.28	...	3.86 ± 1.42	32.7	6.1 ± 2.0	2,3,4
SPT0418-47	0.44 ± 0.21	0.58 ± 0.18	0.22 ± 0.08	0.81 ± 0.34	0.91 ± 0.28	0.39 ± 0.15	18.4	0.73 ± 0.20	2,3,4
SPT0441-46	0.91 ± 0.43	1.21 ± 0.55	0.92 ± 0.34	1.84 ± 0.80	2.00 ± 0.91	1.76 ± 0.66	21.9	2.7 ± 0.8	2,3,4
DLA0817g	1.05 ± 0.55	...	...	1.96 ± 1.03	...	...		1.5 ± 0.9	6
SDP81	1.61 ± 0.69	...	1.39 ± 0.48	2.53 ± 1.15	...	1.76 ± 0.61		3.3 ± 1.1	1,7
AZTEC/C159	1.31 ± 0.63	...	...	3.80 ± 1.84	...	...		1.5 ± 1.2	8
J1000 + 0234	...	...	2.38 ± 0.85	...	...	3.60 ± 1.29		0.94 ± 0.35	1
GN20	10.40 ± 5.54	...	5.47 ± 2.03	18.63 ± 9.89	...	7.73 ± 2.87		0.96 ± 0.38	9,10
ID141	3.68 ± 1.61	3.91 ± 1.08	4.67 ± 1.51	7.59 ± 3.33	5.77 ± 2.52	6.95 ± 2.25		4.9 ± 1.9	11
SPT2132-58	1.99 ± 0.91	1.30 ± 0.54	2.47 ± 0.93	4.26 ± 1.95	2.30 ± 0.97	5.13 ± 1.94	25.3	5.7 ± 1.9	2,3,4
SPT2146-55	1.79 ± 0.85	3.57 ± 1.17	1.87 ± 0.70	3.68 ± 1.72	6.02 ± 1.97	3.66 ± 1.36	26.5	12.9 ± 3.6	2,3,4

Notes:[a]Dust temperature obtained by fitting a modified blackbody to the flux measurements at wavelengths $\geq 500\ \mu$m (see the text). References: 1: This paper; 2: Reuter et al. (2020); 3: Aravena et al. (2016); 4: Bothwell et al. (2017); 5: Coppin et al. (2010); 6: Neeleman et al. (2020); 7: Dye et al. (2015); 8: Jiménez-Andrade et al. (2018); 9: Hodge et al. (2012); 10: Daddi et al. (2009); 11: Dye et al. (2022).

from the best-fitting modified blackbody. For the galaxies for which there is only a flux measurement at a single wavelength, we estimated the rest-frame flux density at 850 μm from this measurement and a modified blackbody with a dust temperature of 25 K and $\beta = 2$.

Where necessary we corrected the line and continuum fluxes for the gravitational magnification factors given in Table 1. We have estimated errors in our metal masses by adding the following errors in quadrature: the error in the calibration factor (see above), the error in the flux of the tracer, and, where applicable, the errors in the gravitational magnification factor and the CO $2-1/1-0$ line ratio. All the galaxies in the sample have observations of at least one tracer, 10 have observations of two tracers, and seven have observations of all three.

3.2 Corrections for the cosmic microwave background

At these redshifts, the cosmic microwave background (CMB) can have a large effect on submillimetre and radio observations, leading to underestimates in both line and continuum flux measurements. We have made corrections to the line and continuum fluxes using the method in da Cunha et al. (2013). In this work, we estimate metal masses both with and without a correction for the CMB because of the potential for errors introduced by the assumptions necessary in making this correction.

For optically thin radiation, which is the case for the dust continuum radiation at long wavelengths and the C I $J = 1 - 0$ line (Harrington et al. 2021; Papadopoulos et al. 2022), the CMB corrections only depend on the temperature of the dust and the excitation temperature of the gas, respectively. For the dust, we corrected the continuum flux densities for each galaxy using equations (12) and (18) in da Cunha et al. (2013) on the assumption that the temperature of the dust if it were not for the CMB would be 25 K (Section 3.1). We then estimated the rest-frame 850-μm flux density from the corrected flux densities using the procedure described in Section 3.1. The excitation temperature of the C I $1 - 0$ line for DSFGs is $\simeq$25 K (Papadopoulos et al. 2022), very similar to our estimates of the dust temperature (Section 3.1), which is what one would expect if the dust temperature and kinetic temperature are the same and the gas is in local thermodynamical equilibrium. For the CI, we therefore assumed the same temperature and used the same equations to make the CMB correction.

The corrections for the CO $J = 1 - 0$ and $J = 2 - 1$ lines are not so obvious since the lines are optically thick, which means the corrections should depend on the opacity of the gas as well as on its temperature (da Cunha et al. 2013). The uncertainties in the corrections from the inclusion of opacity are so large that we decided not to try to include the effect of opacity but to apply the same method as for the optically thin C I line. Our CMB corrections for the CO lines therefore show the possible size of the effect of the CMB, but the actual size of the correction for these lines is very uncertain.

3.3 Results

Table 3 lists our estimates of the mass of metals using the three independent tracers, with and without a correction for the CMB. The results are shown in Fig. 1. The figure shows that there is very good agreement between the masses calculated using the different tracers. For nine out of 10 galaxies, the different mass measurements are consistent within the errors. The only exception is SPT0345-47, for which the estimates from CO and dust are in very good agreement, but both are higher than the 3σ upper limit from the C I $1 - 0$ observation.

The line at the bottom of each panel shows an estimate of the mass of metals in the molecular phase of the ISM in the Galaxy $(1.3 \times 10^7\ M_\odot)$, which we have calculated from an estimate of the mass of molecular gas in the Galaxy of $\simeq 1.1 \times 10^9\ M_\odot$ (Yin et al. 2009) and estimates of the gas-to-dust ratio (167.2) and of the fraction of metals in dust (0.52) from Roman-Duval et al. (2022). The mass of metals in the ISM in these high-redshift galaxies is therefore $\simeq$100-1000 times greater than the mass of metals in the molecular gas in the Galaxy today.

Since it seems likely that the DSFGs are the ancestors of present-day massive early-type galaxies (Section 1), it is interesting to compare the masses of metals for the two populations. A useful low-redshift benchmark is the *Herschel* Reference Survey (HRS), which is a volume-limited sample of galaxies that includes the Virgo Cluster (Boselli et al. 2010; Eales et al. 2017). Since most of the metals in an early-type galaxy are contained in the stars, we have estimated the metal mass for the HRS early-type galaxies from estimates of their

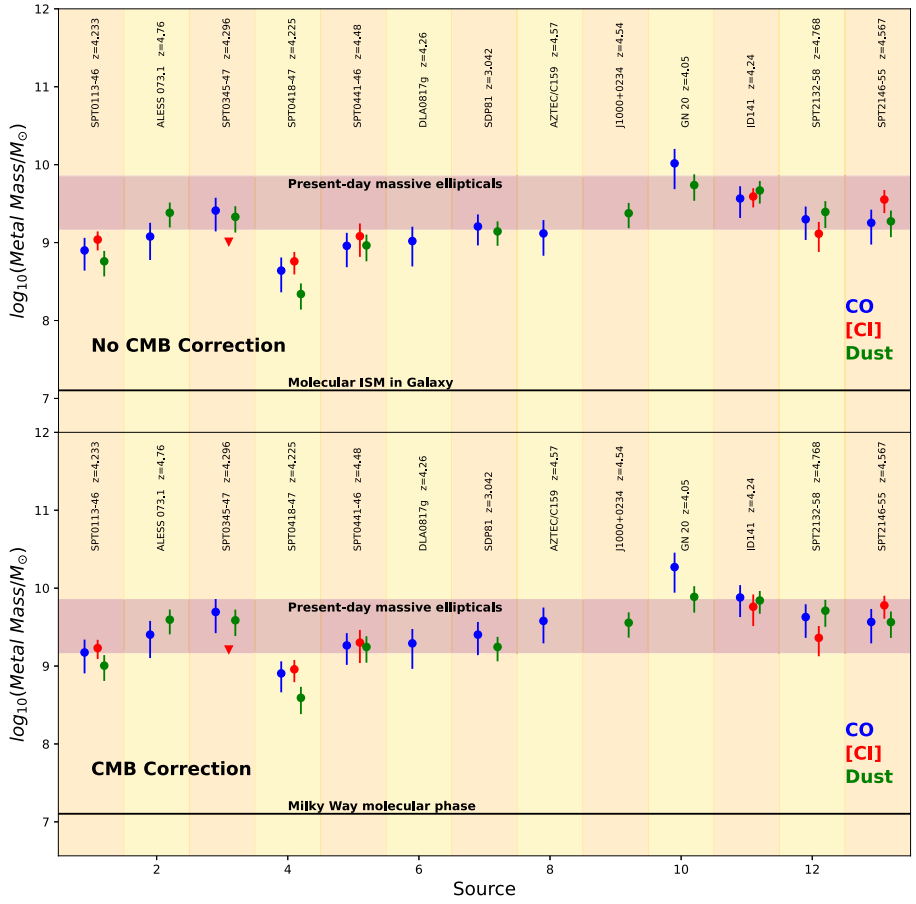

Figure 1. Estimates of the mass of metals in the molecular gas in the 13 DSFGs estimated from CO lines (blue), the C I 1 − 0 line (red) and dust continuum emission (green). The upper panel shows the estimates without a correction for the effect of the CMB, the lower panel the estimates after this correction has been made. The horizontal line shows an estimate of the mass of metals in the molecular gas in the Galaxy today (see text). The horizontal purple band shows an estimate of the range of metal mass for the most massive early-type galaxies in the Universe today (see text).

stellar masses (De Vis et al. 2017) and a stellar metal abundance of $\log_{10}(Z/Z_{\odot}) = 0.3$, appropriate for the galaxies with the highest masses (Gallazzi et al. 2005). In the figure, the purple horizontal band shows the range of metal mass for the HRS early-type galaxies, from the one with the largest stellar mass down to the one with the tenth largest stellar mass. When the correction for the CMB is included (lower panel), the DSFGs contain a mass of metals very similar to that in their probable descendants in the Universe today.

3.4 Limitations of the method

We have used the calibration factors from Dunne et al. (2022), but their values are actually very similar to the other recent best estimates in the literature. Our value for $\alpha_{\rm CO}$ - 4.0 $M_{\odot}$ (K km s^{-1} pc^2)$^{-1}$) is very similar to the value adopted in the latest big review article on the subject: $\alpha_{\rm CO} = 4.36 \pm 0.9$ $M_{\odot}$ (K km s^{-1} pc^2)$^{-1}$ (Tacconi et al. 2020). It is lower than the value of $\alpha_{\rm CO} = 6.5$ $M_{\odot}$ (K km s^{-1} pc^2)$^{-1}$ adopted by Scoville and collaborators (Scoville et al. 2016) but adopting this value would make the metal masses of the DSFGs even higher. Our value for the calibration factor for the dust emission ($1/\alpha_{850\mu{\rm m}} = 6.9 \times 10^{12}$ W Hz^{-1} $M_{\odot}^{-1}$) is very similar to the value adopted in Scoville et al. (2016) ($1/\alpha_{850\mu{\rm m}} = 6.2 \times 10^{12}$ W Hz^{-1} $M_{\odot}^{-1}$). Our value for the calibration factor for atomic carbon ($\alpha_{\rm CI} = 17.0$ $M_{\odot}$ (K km s^{-1} pc^2)$^{-1}$) is also similar to the value found in the most comparable large study (Heintz & Watson 2020): $\alpha_{\rm CI} = 21.4^{+13}_{-8}$ $M_{\odot}$ (K km s^{-1} pc^2)$^{-1}$.

Although our method does not require an assumption about the metal abundance in the galaxy, it still does rely on the same assumption as the widely used method for estimating the mass of molecular gas: that the physical and chemical properties of the ISM on which the calibration factors depend are the same as in the Galaxy.

4 WHAT DO THE DYNAMICAL MASSES TELL US?

4.1 Estimates of the masses

The evidence that the gas in the DSFGs lies in a cold rotating disc is two-fold. First, the DSFGs all have velocity profiles (velocity versus radius) that are very similar to the velocity profiles of rotating disc galaxies in the Universe today. Second, the galaxies mostly have ratios of $v_{\rm rot}/\sigma > 10$, in which $v_{\rm rot}$ is the rotational velocity of the gas and σ its velocity dispersion. Such a high ratio suggests that gravity in the galaxy is being balanced by centripetal force rather than by the internal pressure provided by the spread in stellar velocities. All 13 galaxies have published estimates of their dynamical masses, which are listed in Table 4. In all cases, these have been obtained using modelling packages such as 3DBarolo (Di Teodoro & Fraternali 2015), which make it possible to vary the velocities in concentric

Table 4. Dynamical Masses.

Source	Mass from literature (10^{11} $M_\odot$)	Our Mass estimate (10^{11} $M_\odot$)	Radius (kpc)	Correction for asymmetric drift (per centage)	Reference
SPT0113-46	1.1 ± 0.1	0.93 ± 0.13	3.2	1.0	Rizzo et al. (2021)
ALESS073.1	0.55 ± 0.13	0.89 ± 0.19	3.5	5.0	Lelli et al. (2021)
SPT0345-47	0.40 ± 0.03	0.48 ± 0.08	3.0	8.2	Rizzo et al. (2021)
SPT0418-47	0.25 ± 0.02	0.53 ± 0.08	3.5	2.1	Rizzo et al. (2020)
SPT0441-46	0.32 ± 0.02	0.48 ± 0.09	2.0	1.4	Rizzo et al. (2021)
DLA0817g	0.91 ± 0.29	0.90 ± 0.19	4.2	26	Neeleman et al. (2020)
SDP81	0.38 ± 0.06	0.41 ± 0.08	1.5	9.8	Dye et al. (2015)
AZTEC/C159	1.4 ± 0.7	1.8 ± 1.1	3.0	0.2	Fraternali et al. (2021)
J1000 + 0234	2.3 ± 0.3	2.7 ± 0.3	4.0	0.8	Fraternali et al. (2021)
GN20	6.4 ± 2.8	6.3 ± 1.5	7.0	18	Hodge et al. (2012)
ID141	1.0 ± 0.5	0.95 ± 0.29	2.0	2.0	Dye et al. (2022)
SPT2132-58	0.39 ± 0.04	0.38 ± 0.08	4.0	1.3	Rizzo et al. (2021)
SPT2146-55	0.22 ± 0.02	0.23 ± 0.04	2.7	2.0	Rizzo et al. (2021)

rings around the centre of the galaxy, and also the position of the centre and the inclination and position angle of the disc, until the model provides a good fit to the spectroscopic data.

For six of the 13 galaxies, the authors of the mass estimate have made an explicit correction for the effect of the stellar pressure, the 'asymmetric drift'. In the other studies, the authors have simply assumed it is negligible because of the high ratio of v_{rot}/σ. For each of the galaxies, we have used the data in the original papers to estimate the relative contributions of the asymmetric drift and the centripetal force, and where necessary made a correction to the published masses (Appendix B). For all but two galaxies the correction to the mass is $\leq$10 per cent.

The original papers sometimes list separate estimates of the baryonic and non-baryonic masses (where they have done this we list the former in Table 4). In order to check that there are no systematic errors in the original analysis, we have made our own estimates of the total dynamical masses from the velocity profiles and the estimates of the galaxy inclination in the original papers.

We made our estimates of the mass from the equation

$$M_{\rm tot} = \frac{v^2 r}{G \sin(i)^2}, \tag{3}$$

in which v is the rotational velocity of the gas at a distance r from the centre of the galaxy and i is the estimate of the inclination of the disc. We have made a correction to these estimates for the effect of asymmetric drift (Appendix B). Equation (3) gives the correct mass interior to r if the density distribution is spherically symmetric. If the density is not spherically symmetric our mass estimates will be too high (Walter et al. 1997) – by roughly 40 per cent if the mass is distributed in a razor-thin exponential disc.[1] We calculated errors in the mass estimates by combining the errors in velocity and inclination. Table 4 lists our mass estimates and the distance from the centre of the DSFG at which we made the estimate.

The published mass estimates and own estimates are in good agreement for 10 out of the 13 galaxies, which agrees with the evidence that non-baryonic matter is negligible in the central regions of high-redshift galaxies (Genzel et al. 2017). For the three galaxies where there is a significant discrepancy, our mass estimate is higher than the published mass by a factor of 1.6 for ALESS073.1, by a factor of 2.1 for SPT0418-47 and by a factor of 1.5 for SPT0441-46.

[1]Bovy 2022.

4.2 The mass of the molecular gas versus dynamical mass

We estimated the mass of the molecular gas in each galaxy using equation (1) rather than equation (2) but otherwise followed the procedure described in Section 3.1, which means our mass estimates are equal to the metal mass estimates in Table 3 multiplied by the gas-to-metal ratio (86.9). Since the dynamical masses we have measured ourselves are slightly larger than the ones in the literature, and therefore place a less stringent upper limit on the mass of molecular gas, to be conservative we have used our mass estimates rather than the published ones.

Ideally, we would compare the dynamical mass with an estimate of the mass of molecular gas made within the same radius used to estimate the dynamical mass. This is possible for the observations of the dust, for which there are high-resolution observations that show the emission is coming from within the radius listed in Table 4 (Daddi et al. 2009; Dye et al. 2015; Spilker et al. 2016; Dye et al. 2022). However, most of the CO and C I observations (Aravena et al. 2016; Bothwell et al. 2017) do not have enough resolution to show definitively whether the CO and C I emission is coming from within the region covered by the dynamical analysis. In the case of the CO observations, this is because of the lack of a telescope with enough resolution and in the case of the CI this is because of the need for impractically long integration times with ALMA.

Nevertheless, there is a high-resolution map of C I 1 – 0 for one galaxy (Dye et al. 2022) and there is one galaxy that has a large enough angular size that CO 1–0 observations have enough resolution (Hodge et al. 2012). In both galaxies, the line emission from the tracer does come from within the region covered by the dynamical analysis. Furthermore, detailed radiative modelling of multiple CO and C I lines from 24 high-redshift DSFGs (Harrington et al. 2021) suggests that the emission in these lines is typically from a region within 3 kpc of the centre of the galaxy, very similar for most of the galaxies to the radius of the region covered by the dynamical analysis (Table 4). However, we cannot say for certain that in all 13 galaxies the C I and CO emission is confined to the region covered by the dynamical analysis.

Fig. 2 shows the comparison between the dynamical mass and the mass of the molecular gas. The dynamical mass is a measure of the total mass, which is the sum of the masses of all the galaxy's components: gas, stars, and non-baryonic matter. But Fig. 2 shows that for many of the galaxies the estimate of the mass of the gas is actually higher than the estimate of the total mass. This paradox has

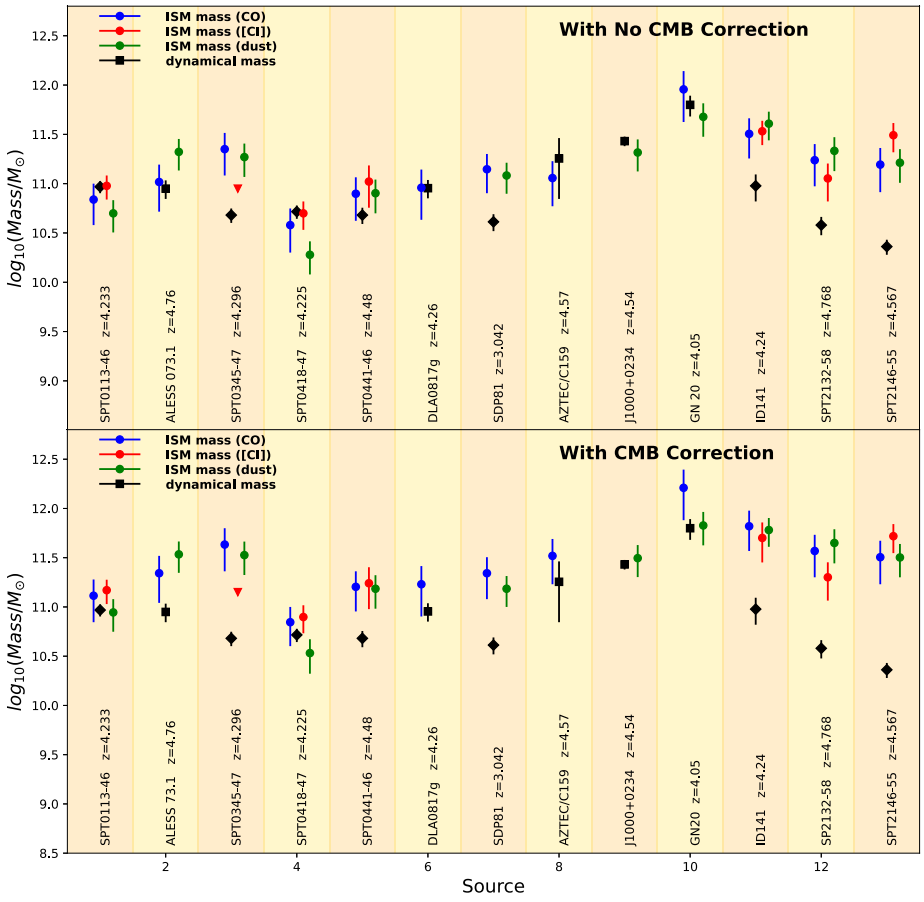

Figure 2. A comparison of the dynamical mass of each DSFG with an estimate of the mass of its gas made using three different tracers: carbon monoxide (blue), atomic carbon (red), and dust grains (green). The estimate of the dynamical mass is shown by a black diamond if the source is gravitationally lensed and a black square otherwise. The upper panel shows the estimates of the gas mass with no correction for the CMB, the lower panel shows the estimates after this correction has been made (see the text).

been spotted many times before when CO has been used as a tracer, but the figure shows that there is the same problem when C I and dust are used. There is, of course, the caveat that, as we noted above, for many of the galaxies we cannot be sure that the C I and CO emission is confined within the region covered by the dynamical analysis, but we note that the discrepancies when dust is used as a tracer are just as large as for the other two tracers. Moreover, the galaxy for which there is a high-resolution map in C I1-0, ID141 (Dye et al. 2022), is one of the best examples of this paradox.

4.3 Possible solutions of the paradox

This paradox has been noted many times before in papers in which CO has been used to estimate the gas mass. Our results show that the same problem is present when carbon atoms and dust grains are used. Unless the assumptions used in the dynamical estimates are completely wrong, or the emission from the tracer is mostly from outside the region covered by the kinematic observations (Section 4.2), the only way to make the gas masses consistent with the dynamical masses is to reduce the values of the three calibration factors.

A crucial point to note when thinking about this issue is that the good agreement between the gas mass estimates made with the different tracers implies that if the calibration factors are lower than the Galactic values, all three must be lower by a similar factor. This conclusion is supported by the analysis in Dunne et al. (2022) of 407 galaxies in the redshift range $0 < z < 5$. By examining the ratios of the luminosity of the emission from the three tracers, these authors concluded that there was no difference in the ratios of the calibration factors between normal galaxies and DSFGs and between DSFGs at $z < 3$ and $z > 3$.

There are two possible explanations of why the calibration factors for the DSFGs might be lower than the Galactic values. The first is that the difference is caused by some differences between the ISM in the galaxy and in the Galaxy in the critical properties on which the calibration factors depend. The explanation that is commonly made for a low value of $\alpha_{\rm CO}$, for example, is that the molecular gas in a DSFG has a higher temperature and lower density than in the Galaxy (Downes & Solomon 1998). In Appendix A, we consider the properties of the ISM that might lead to a change in the calibration factor. For each tracer, there is one plausible difference between the ISM in a high-redshift DSFG and the Galactic ISM that might lead to a change in the calibration factor.

In the case of CO, the obvious possibility, suggested by the high star-formation rate in these galaxies, is that the ISM in a high-redshift DSFG is warmer and less dense than the Galactic ISM, which would lead to a lower value of α_{CO}. The original motivation for this suggestion were some CO observations which suggested that this is the case in two low-redshift DSFGs (Downes & Solomon 1998). It is worth noting, however, that the results from the first

comprehensive multi-line investigation of CO in a large sample of high-redshift DSFGs Harrington et al. (2021) suggest that the ISM in these galaxies is not dominated by a low-density component. The authors of this study concluded that much of the CO in the high-redshift DSFGs is in warm dense gas, which they argued would have been missed by the observations in the low-J CO transitions used to observe the two low-redshift DSFGs (Harrington et al. 2021), leading to an estimate of the value of $\alpha_{\rm CO}$ in the earlier study that was too low.

In the case of C I, the most plausible possibility, suggested by the high star-formation rates in these galaxies, is that an increase in the density of cosmic rays leads to a change in the carbon chemistry, increasing the abundance of C I relative to CO (Bisbas, Papadopoulos & Viti 2015; Glover & Clark 2016; Gong et al. 2020; Bisbas, Tan & Tanaka 2021; Dunne et al. 2022) and decreasing the value of $\alpha_{\rm CI}$.

In the case of the dust, there are several ways that the dust grains might differ from those in the Galaxy: in their chemical composition, structures, sizes, and shapes, all of which might change the value of the calibration factor (Clark et al. 2016). The obvious way to make the value of the calibration factor lower in a DSFG is if the sizes of the grains there are generally smaller than in the Galaxy.

The essential problem with this explanation is that each of the three calibration factors depends on very different properties of the ISM. Even if there was any evidence that the critical properties of the ISM on which the calibration factors depend are different in high-redshift galaxies, which isn't the case even for CO (Harrington et al. 2021), it would be a remarkable coincidence if they were different in such a way that the calibration factors for all three tracers were reduced by the same amount.

The second simpler explanation is that the metal abundance in the DSFGs is higher than in the Galaxy today. This provides a straightforward explanation of why the calibration factors for dust and C I are lower by the same factor because the emission from both is optically thin and inversely proportional to metal abundance. It is not a perfect explanation because the relationship between the optically thick CO emission and metal abundance is more uncertain, but a compilation of the data is at least consistent with a similar relationship to that for the other two tracers (Bolatto et al. 2013; see their fig. 9), and if so the calibration factor for the CO would decrease in the same way as for the other two tracers.

For the rest of this paper, we will follow Occam's Razor and assume that the second explanation is the correct one, although we cannot rule out the first. If we are wrong and the calibration factors are lower by a factor of X because of differences in the physics/chemistry/structure of the ISM/dust grains, our estimates of the metal masses in Section 3 will be too high by the same factor.

4.4 Metal abundances

We have estimated a lower limit to the metal abundance of each galaxy from the equation:

$$\frac{Z}{Z_\odot} > \frac{M_{\rm metals}}{M_{\rm dyn} \times 0.0142} \tag{4}$$

in which $M_{\rm metals}$ is our estimate of the mass of the metals, in which the corrections for the CMB have been included, $M_{\rm dyn}$ is the dynamical mass, and the number on the right-hand side is the bulk metal fraction of the Sun (Asplund et al. 2009). Our estimates of the limits on Z, which range from $0.9Z_\odot$ to $12.9Z_\odot$, are listed in Table 3 and a histogram of the values is shown in Fig. 3.

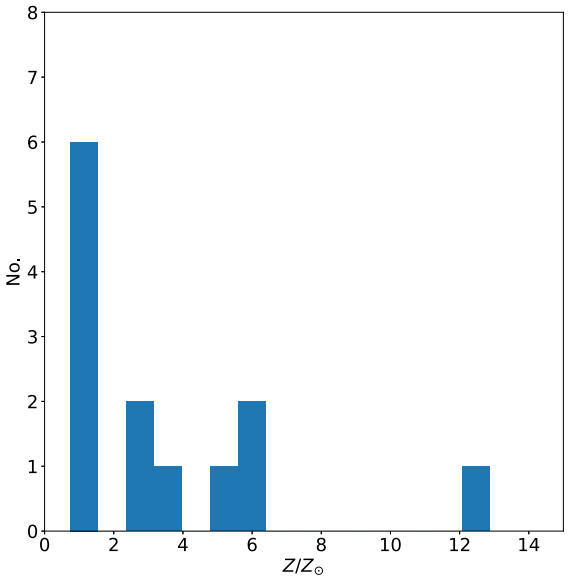

Figure 3. Estimates of the lower limit on the metal abundance for the 13 galaxies (Section 4.4).

There are estimates of the metal abundances in the literature for three of our targets. The previous estimates and our lower limits are consistent for two galaxies but not for the third. For ALESS073.1 the previous estimate, from far-infrared spectral lines, is that $Z/Z_\odot$ is in the range 0.6–3 (De Breuck et al. 2014), which is consistent with our lower limit of 2.5 ± 0.9. For SPT0418−47, the previous estimates, from far-infrared line measurements ($0.3 < Z/Z_\odot < 1.3$, De Breuck et al. (2019)) and from JWST spectroscopy ($Z/Z_\odot \simeq 1.6$, Peng et al. (2023), are consistent with our lower limit ($Z/Z_\odot > 0.73 \pm 0.2$. The inconsistency is for SDP81. There are two estimates from far-infrared spectral lines: $Z/Z_\odot < 2$ (Rigopoulou et al. 2018) and $Z/Z_\odot \simeq 0.5$ (Rybak et al. 2023). The second at least is inconsistent with our lower limit: $Z/Z_\odot > 3.3 \pm 1.1$.

5 METALS INSIDE AND OUTSIDE GALAXIES-CHEMICAL EVOLUTION MODELS

Such high metal masses and metal abundances at such early times are perhaps surprising because there would have been much less time to make the metals. We have used two chemical-evolution models to investigate whether it is possible to make such large masses of metals so quickly.

The first is the widely used gas-regulation model (Lilly et al. 2013; Peng & Maiolino 2014). In this model, there is a flow of gas from the intergalactic medium into the galaxy, and there is also an outflow with a rate proportional to the galaxy's star-formation rate, which leads eventually to the mass of the ISM reaching an equilibrium value. The mass of metals that are produced in this model depends on the strength of the outflow and the form of the stellar initial mass function (IMF).

The gas-regulation model is based on the 'instantaneous recycling approximation', in which it is assumed that all the metals produced by a newly formed population of stars are made the moment the stars are born and immediately released into the ISM. This assumption is likely to be a poor one for high-redshift DSFGs because of their very short gas depletion times (Dye et al. 2015, 2022). We have therefore also included the predictions of a model that does not include this assumption, which we constructed to model the evolution of one

of the galaxies in our sample (Dye et al. 2022). This model also includes more realistic inflows and outflows and takes account of the dependence of stellar yields on metal abundance.

5.1 The gas-regulation model

In this model, there is an outflow with a rate equal to a constant (Λ) times the galaxy's star formation rate, which leads to the mass of the ISM eventually reaching an equilibrium value (hence the term 'gas regulation'). We use the analytic formalism of Peng & Maiolino (2014), which makes it possible to follow the evolution of a galaxy from $t = 0$ to $t >> \tau_{\rm eq}$, when the galaxy asymptotically approaches an equilibrium state. In this equilibrium state, the gas mass, the metal abundance in the gas, and the mass of metals in the gas are constants, although the mass of stars continues to rise as new stars are born.

The equilibrium time, $\tau_{\rm eq}$ is given by

$$\tau_{\rm eq} = \frac{\tau_{\rm dep}}{1 - R + \Lambda} = \frac{1}{\epsilon(1 - R + \Lambda)} \tag{5}$$

in which $\tau_{\rm dep}$ is the depletion time (the ratio of the gas mass to the star-formation rate), ϵ is the inverse of this (the star formation efficiency), and R is the fraction of the mass of a cohort of newly formed stars that are eventually returned to the ISM, which in the instantaneous recycling approximation happens immediately. We have expressed the time dependence of our models in units of the equilibrium time so they apply to all galaxies and do not vary with the values of ϵ, R, and Λ in individual galaxies.

We have used the following equations taken directly from Peng & Maiolino (2014):

$$M_{\rm gas} = \frac{\Phi}{\epsilon(1 - R + \Lambda)} \left(1 - e^{-\frac{t}{\tau_{\rm eq}}} \right) \tag{6}$$

$$M_{\rm star} = \frac{\Phi}{\epsilon} \frac{1 - R}{(1 - R + \Lambda)^2} \left[\frac{t}{\tau_{\rm eq}} - \left(1 - e^{-\frac{t}{\tau_{\rm eq}}} \right) \right] \tag{7}$$

$$Z_{\rm gas} = \frac{y}{1 - R + \Lambda} \left(1 - e^{-\frac{t}{\tau_{\rm eq}}} \right) \left[1 - e^{-\left(\frac{t}{\tau_{\rm eq}(1 - e^{-\frac{t}{\tau_{\rm eq}}})} \right)} \right] \tag{8}$$

In these equations, y is the yield, the mass of metals produced by one solar mass of stars, and Φ is the rate at which gas is flowing onto the galaxy. We can combine equations (6) and (8) to get an estimate of the total mass of metals in the ISM:

$$M_{\rm metals} = Z_{\rm gas} M_{\rm gas} \tag{9}$$

We then combine equations (6), (7), and (9) to calculate the ratio of the metal mass to the total mass ($M_{\rm gas} + M_{\rm star}$). Neither this ratio nor the metal abundance of the ISM (equation 8) depends on the values of Φ or ϵ but they do depend on the values of R, y, and Λ. The first two of these depend on the choice of the IMF.

5.2 A bespoke model

The instantaneous recycling assumption may be particularly poor for high-redshift DSFGs because of their very short gas-depletion and dynamical times (Dye et al. 2015, 2022). We have therefore also used a chemical evolution model we developed for the z = 4.24 DSFG ID141, which does not include this assumption and which incorporates the lifetimes of the stars that make the metals (Dye et al. 2022). We refer the reader to our earlier paper for more details of the model but, in brief, the galaxy starts as a cloud of gas with no heavy elements, with the gas then being converted into stars using an assumed IMF and star-formation history. Outflows of gas and metals are based on prescriptions of feedback from stars and active galactic nuclei, and the model includes inflows via accretion from the cosmic web. Stars eject gas, metals, and dust in each generation based on prescriptions for the stellar yield of low-mass (van den Hoek & Groenewegen 1997) and high-mass stars (Maeder 1992) and for the remnant mass function (De Vis et al. 2021).

Table 5. Our assumptions about the return fraction and yield.[a]

IMF	Yield (y)	Return fraction (R)
Salpeter	0.023	0.24
Chabrier	0.040	0.38
Top-heavy (Cappellari et al. 2012)	0.088	0.80
Top-heavy (Zhang et al. 2018)	0.085	0.65

[a] We use the definition of yield in Peng & Maiolino (2014).

5.3 Results

We have considered four different forms for the IMF. The first two are the commonly used Chabrier and Salpeter IMFs. The other two are top-heavy IMFs in which there is a higher proportion of high-mass stars. One of these was proposed to explain the dynamics of low-redshift elliptical galaxies (Cappellari et al. 2012), the other to explain the observations of isotopologues of carbon monoxide in four DSFGs (Zhang et al. 2018). We have estimated the values of the return fraction, R, and the yield, y, for each IMF from a compendium of stellar yields (Nomoto, Kobayashi & Tominaga 2013). The values are listed in Table 5.

The predictions of both models for the ratio of metal mass to total mass (gas plus stars) versus time are shown in Fig. 4 and the predictions for metal abundance versus time in Fig. 5. Time is plotted in units of the equilibrium time, a key parameter of the gas-regulation model, along the top of each figure. To give an impression of the timescales, we have calculated the value of $\tau_{\rm eq}$ in years using a Chabrier IMF and the properties of the galaxy ID141 (Dye et al. 2022), and then plotted time in the usual units along the bottom of the figures, although strictly this is only correct for one galaxy and one form of the IMF. We stopped the model based on ID141 (Dye et al. 2022) when it reached a stellar mass of 5×10^{11} $M_\odot$ when we assume an outflow clears the galaxy of its ISM (Romano et al. 2017). The left panel in each figure shows the predictions for the standard Chabrier and Salpter IMFs and the right panels show the predictions for the top-heavy IMFs.

In Fig. 4, we have compared the predictions of the models to our estimates of the ratio of metal mass to total mass for the DSFGs. In making these estimates, we have assumed that the total mass is given by the dynamical mass. In Fig. 5, we have compared the model predictions to our estimates of the lower limits on the metal abundance, which are listed in Table 3. Since the ages of the galaxies are unknown, we have plotted our estimates for the DSFGs in both figures at arbitrary points along the time axis. Note that our estimates for the DSFGs in the two figures have a simple scaling. The difference in the two figures is that in Fig. 4 we are using the models to predict the ratio of mass of metals in the gas to the total mass (gas plus stars) and in Fig. 5 we are using the models to predict the metal abundance in the gas.

Fig. 4 shows that the predictions of both models are very similar, with the only difference being, as expected, that the ratio of metal

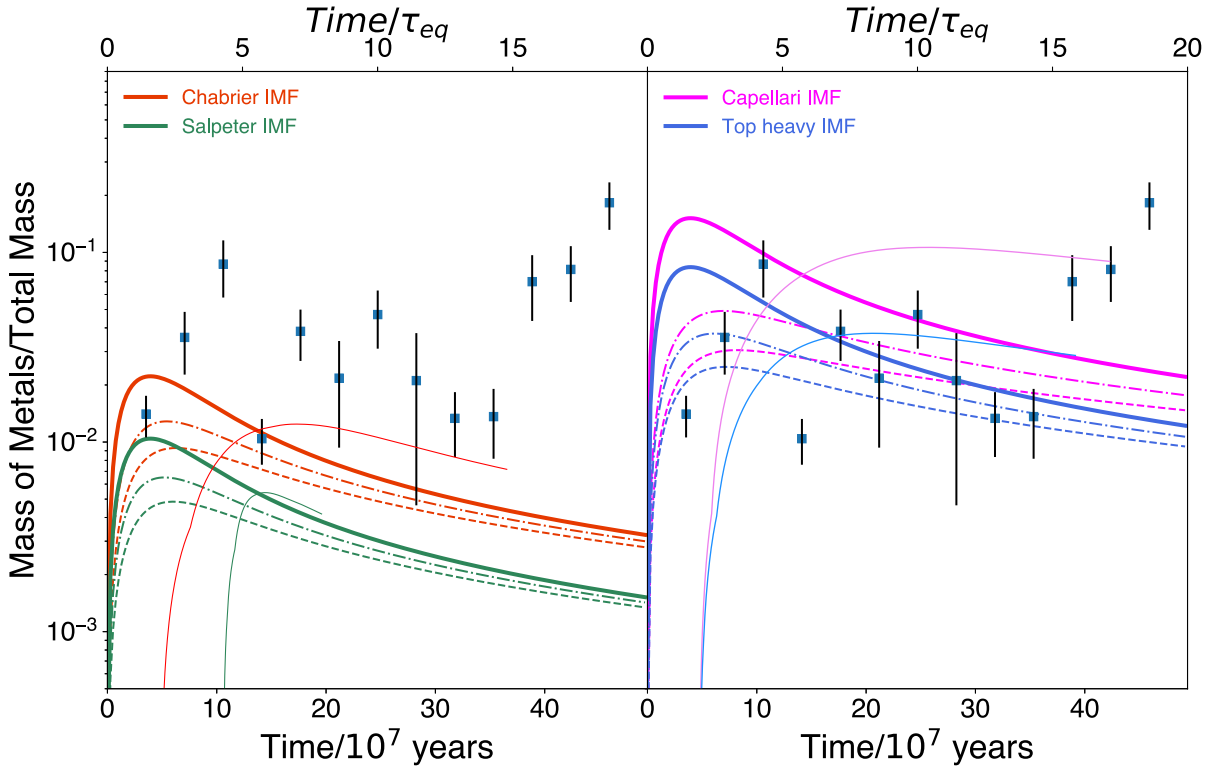

Figure 4. The ratio of the mass of ISM metals to the total galaxy mass (gas plus stars) plotted against time. The squares show our estimates for the 13 DSFGs, which, since we don't know their ages, are plotted at arbitrary positions along the time axis. The thick lines show the predictions of the gas-regulation model, in which metals are instantaneously ejected into the ISM. The thin lines show the predictions of a model that includes the delay in metal production that arises from the lifetimes of the stars. The left panel shows the predictions for two standard IMFs (Chabrier and Salpeter) and the right panel for two IMFs with a larger proportion of high-mass stars (Cappellari et al. 2012; Zhang et al. 2018) (key at top of each panel). The continuous, dot-dashed, and dashed lines show the predictions for different outflow parameters: $\Lambda = 0, 1, 2$, respectively. Time is expressed in units of the equilibrium time used in the gas-regulation model along the top of the figure and in years along the bottom of the figure (see the text).

mass to total mass peaks later for the model that includes a delay from stellar lifetimes. Nevertheless, even in this model, the peak is reached very early, only $\simeq 2 \times 10^8$ years after the galaxy begins to form, much less than the time since the big bang at these redshifts.

The left-hand panel of Fig. 4 shows that the model predictions for metal mass over total mass for the two standard forms of the IMF are too low compared with our estimates of this ratio for the DSFGs. In the case of metal abundance, the left-hand panel of Fig. 5 shows that it is possible to reproduce our estimates of metal abundance (actually lower limits on metal abundance) for a standard IMF and a closed-box model, although not so well if there is an outflow. A closed-box model, however, seems implausible given the evidence for outflows from star-forming galaxies in the high-redshift Universe (Spilker et al. 2018; Jones et al. 2019; Ginolfi et al. 2020; Veilleux et al. 2020).

The right-hand panels in both figures show that with a top-heavy IMF the model predictions agree much better with our estimates. We note that although we don't know the ages of these galaxies, it seems likely that we are seeing them at an epoch at which the dust mass, and therefore the mass of metals in the ISM, was at close to its maximum value, simply because of the strong selection bias towards high dust masses for the galaxies discovered in a submillimetre survey.

The curves in both figures for both sets of models are sensitive to the choice of input yields and the chosen remnant mass function (which in turn affects the return fraction R). Different stellar yield tables (Karakas et al. 2018; Limongi & Chieffi 2018), for example, can reduce the yield, y, and hence the metal abundance, $Z_{\rm gas}$, by 20–30 per cent for the Cappellari IMF (Cappellari et al. 2012). This is not enough to affect the conclusions above.

5.4 The metals in the intracluster gas

Our analysis shows that the DSFGs contain very large masses of metals. There is plenty of evidence for massive outflows of gas from high-redshift DSFGs (Spilker et al. 2018; Jones et al. 2019; Ginolfi et al. 2020; Veilleux et al. 2020), suggesting that a significant proportion of the metals produced in the galaxies should have been ejected into intergalactic space. In this section, we will investigate the possibility that these ejected metals might be the solution to the long-standing conundrum that $\simeq$75 per cent of the metals in rich clusters of galaxies are in the intergalactic gas rather than in the galaxies themselves (Loewenstein 2013; Renzini & Andreon 2014).

We have investigated this possibility by extending the gas-regulation model (Section 5.1). On the assumption that the metal abundance in the outflowing gas is the same as in the ISM in the galaxy, the mass of metals ejected into intergalactic space is given by:

$$M_{\rm ejected\ metals} = \int_0^{t_{\rm final}} Z_{\rm gas}\,\Lambda {\rm SFR}\,{\rm d}t \qquad (10)$$

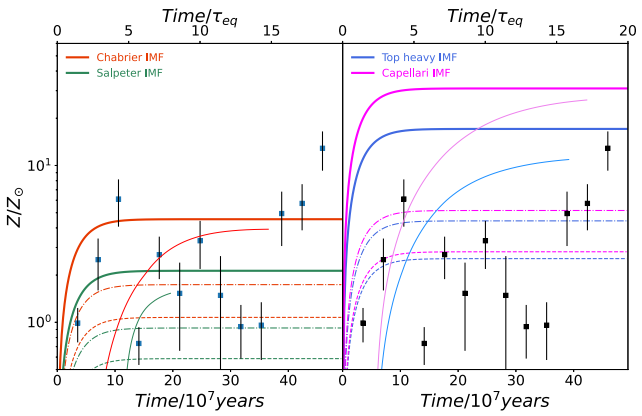

Figure 5. Metal abundance of the ISM plotted against cosmic time. The squares show our estimates of this for the 13 DSFGs (Table 3), which, since we don't know their ages, are plotted at arbitrary positions along the time axis. The thick lines show the predictions of the gas-regulation model, in which metals are instantaneously ejected into the ISM. The thin lines show the predictions of a model that includes the delay in the metal production that arises from the lifetimes of the stars. The left panel shows the predictions for two standard IMFs (Chabrier and Salpeter) and the right panel for two IMFs with a larger proportion of high-mass stars (Cappellari et al. 2012; Zhang et al. 2018) (key at top of each panel). The continuous, dot-dashed and dashed lines show the predictions for different outflow parameters: Λ = 0, 1, 2, respectively. Time is expressed in units of the equilibrium time used in the gas-regulation model along the top of the figure and in years along the bottom of the figure (see the text).

in which SFR is the star-formation rate, which is given by:

$$\mathrm{SFR} = \frac{\Phi}{1 - R + \Lambda}(1 - e^{-\frac{t}{\tau_{\mathrm{eq}}}}) \tag{11}$$

The predicted mass of metals that is incorporated in the stars within a galaxy is given by:

$$M_{\mathrm{metals,\ stars}} = (1 - R)\int_0^{t_{\mathrm{final}}} Z_{\mathrm{gas}}\mathrm{SFR}\,\mathrm{d}t \tag{12}$$

The predicted metal abundance of the stars is then given by:

$$Z_{\mathrm{stars}} = \frac{\int_0^{t_{\mathrm{final}}} Z_{\mathrm{gas}}\mathrm{SFR}\,\mathrm{d}t}{\int_0^{t_{\mathrm{final}}} \mathrm{SFR}\,\mathrm{d}t} \tag{13}$$

Fig. 6 shows a comparison with the observations of the predictions of this model for the metal abundance in present-day cluster galaxies and for the ratio of the mass of metals that is in the cluster gas to the mass of metals that is in the galaxies in the cluster. The metal abundance is given by equation (13), the ratio of the metal masses by equations (10) and (12). The mass ratio is independent of t_{final} and the metal abundance is only weakly dependent on it – we have set its value to 20 τ_{eq}. We have plotted the predictions for outflows with Λ of 1 and 2, typical of the values for high-redshift DSFGs (Ginolfi et al. 2020), and for the four forms of the IMF. The horizontal purple band shows the observed range of the metal ratio for present-day rich clusters (Renzini & Andreon 2014) and the two vertical lines show solar metal abundance (Asplund et al. 2009) and twice solar metal abundance, which is typical of the massive early-type galaxies in clusters (Gallazzi et al. 2005). Several of the models predict values in roughly the right area, showing that the outflow of metals from high-redshift DSFGs is a quantitatively plausible solution of this puzzle.

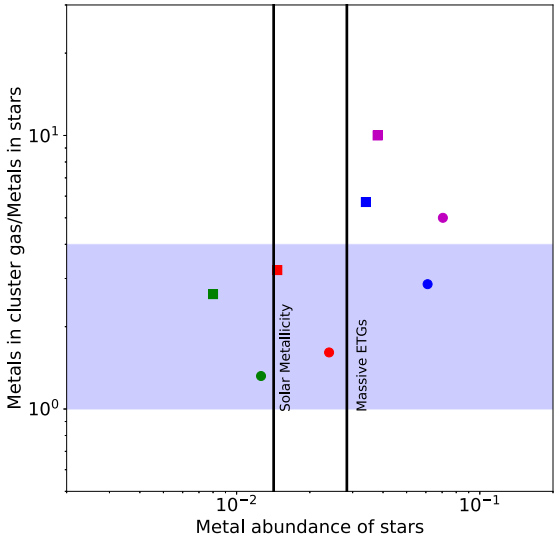

Figure 6. The ratio of the mass of metals in the gas in present-day rich clusters to the mass of metals in the cluster galaxies versus the metal abundance in the galaxies. The horizontal purple band shows the observed range for the mass ratio (Renzini & Andreon 2014). The vertical lines show solar metal abundance (Asplund et al. 2009) and twice solar metal abundance, typical of the massive early-type galaxies in cluster today.The coloured symbols show the prediction of eight models: blue—top-heavy IMF (Zhang et al. 2018); red—Chabrier IMF; purple—top-heavy IMF (Cappellari et al. 2012); green—Salpeter IMF; circles - Λ = 1; squares - Λ = 2.

6 DISCUSSION

6.1 The observational results

We have two main observational results: (1) the mass of metals in the molecular gas in a high-redshift DSFG is very high, as large as the entire metal content of a massive low-redshift early-type galaxy; (2) the metal abundance is also very high, often well over the solar value. In this section, we will discuss the limitations of these results. In the following section we will discuss their implications for galaxy evolution.

The first result seems robust. It is based on the estimates of the calibration factors of the CI, CO, and dust tracers made by Dunne et al. (2022), but these are quite similar to the other recent estimates in the literature (Section 3.4). The discrepancies between the ISM and dynamical mass estimates in Fig. 2 imply that the true calibration factors for the high-redshift DSFGs must be lower than these values, but as long as this decrease is caused by an increase in the metal abundance rather than physical/chemical/structural changes in the ISM/dust, our estimates of the metal mass are unaffected (Section 4.3).

For the second result, there are two causes for concern. The first is the accuracy of the dynamical masses. Although we have checked the published masses by making our own estimates, both sets do rely on the assumption that the gas is distributed in a cold rotating disc. Although the velocity profiles do look remarkably like the rotation curves of present-day disc galaxies (see, for example, the high-resolution velocity profile for SDP81 in Dye et al. 2015), it is possible that these may yet prove to have an alternative explanation.

A more immediate concern is that we cannot be always sure the CO and CI emission is from within the region traced by the dynamical analysis. There have been some recent claimed detections of molecular gas in the haloes around high-redshift AGN (Jones

et al. 2023; Scholtz et al. 2023), which, if it was also true of the DSFGs, would reduce the conflict between the ISM and dynamical mass and weaken the limit on the metal abundance. To estimate the possible size of this effect, we used the results of Scholtz et al. (2023), who used a stacking analysis to search for extended emission in the C I2 − 1 line around a sample of extremely red quasars. They estimated average molecular masses of $10^{10.8\pm0.14}$ $M_\odot$ and $10^{10.2\pm0.16}$ $M_\odot$ for the galaxy and halo components, respectively. If these proportions were also true of the DSFGs, our limits on metal abundance would be lower by $\simeq$20 per cent, although our estimates of the total metal masses would be unaffected.

6.2 Implications for galaxy evolution

The metal abundance in galaxies are generally less at high redshifts, with the metal abundance of a galaxy at $z \sim 4$ being a factor of $\simeq 4$ lower than a galaxy of the same stellar mass in the Universe today (Cullen et al. 2019). There is already evidence in the literature that the high-redshift DSFGs are an anomaly, with most estimates of the metal abundance being at roughly solar or above (De Breuck et al. 2014; Wardlow et al. 2017; Rigopoulou et al. 2018; De Breuck et al. 2019; Peng et al. 2022; Rybak et al. 2023). Our results support this conclusion.

We have used chemical-evolution models to show that it is possible to produce such high metal masses and metal abundances shortly after the formation of a galaxy (Section 5). In these models, the mass of metals in the ISM is at its highest only $\sim 2 \times 10^8$ years after the galaxy begins to form, much less than the age of the Universe at these redshifts. The high values for the ratio of metal mass to total mass (Fig. 4) and for metal abundance (Fig. 5) can only be reproduced by the models if the IMF has a higher fraction of high-mass stars than the standard IMFs. Observations of CO isotopologues in four DSFGs also imply these galaxies have a top-heavy IMF (Zhang et al. 2018).

We used these models to show that the metals in the outflows are a possible explanation of the metals in the gas in present-day clusters (Section 5.4). Fig. 6 shows that this conclusion does not require a top-heavy IMF; the success of the models is due to the large masses of metals carried by the outflows rather than the metal abundance, which is the result that requires a top-heavy IMF. Our model is, of course, very simple, and we have applied it to a sample of extreme DSFGs, which are likely to be the ancestors of only the most massive early-type galaxies. A conclusive demonstration that the metals in galactic outflows are the source of the metals in the intracluster gas would require the model to include galaxies covering the whole range of stellar masses seen in present-day clusters.

Our estimates of the metal abundance in the high-redshift DSFGs are surprisingly large, often even larger than the values for the galaxies that are likely to be their descendants, the most massive early-type galaxies in the Universe today, which have a metal abundance about twice solar (Gallazzi et al. 2005). Is there a way that the subsequent evolution of the DSFG might have reduced its initial metal abundance? The evolutionary route from a DSFG, a galaxy with a small physical size but with a huge star-formation rate, to a massive early-type galaxy in the Universe today, a galaxy with a large physical size but a low star-formation rate, is still very uncertain (Tacchella et al. 2016). We speculate that it is the sequence of mergers that must have occurred to increase the size of the galaxy that has reduced its initial metal abundance. Since models of the stellar populations of present-day early-type galaxies imply that relatively few stars were formed after the DSFG epoch (Thomas et al. 2010), it seems likely that most of these mergers would have been dry mergers, with the DSFG-descended galaxy always being the most massive member of the merger because otherwise its mass would have grown too much by the present day. Given the strong relationship between metal abundance and stellar mass seen at all epochs (Section 1), it therefore seems likely that each merger would have further reduced the metal abundance.

7 CONCLUSIONS

We have estimated the mass of metals in the molecular gas in 13 dusty star-forming galaxies (DSFGs) at $z \sim 4$ for which previous observations have shown that the gas lies in a cold rotating disc. We estimated the metal masses using observations of CO in either the J = 1 − 0 or J = 2 − 1 lines, observations of atomic carbon in the C I1 − 0 line and continuum observations of dust. In making our estimates, we used the first mutually consistent estimates of the calibration factors for the three tracers (Dunne et al. 2022). There were observations of at least two tracers for 10 out of 13 galaxies and observations of all three for 7 galaxies. Our method is independent of the metal abundance in the galaxy, in contrast to the widely used method in which the tracer is used to estimate the ISM mass. We obtained the following results:

(i) We obtained very similar mass estimates from the different tracers, our estimates being similar to the entire metal content of a massive present-day early-type galaxy.

(ii) When we estimated the mass of the ISM rather than the mass of the metals, we found that our estimate was often higher than the estimate of the dynamical mass. This paradox has been noticed before for CO, but the same is true when carbon atoms or dust grains are used as the tracer.

(iii) We argue that the most likely solution of this paradox is that the metal abundances in the high-redshift DSFGs are often higher than in the Galaxy. The alternative explanation, that the calibration factors are lower because of differences in the physics/chemistry/structure of the ISM/dust, seems unlikely because these differences would have to conspire to reduce all three calibration factors by the same amount.

(iv) On the assumption that our solution is the correct one, we estimated lower limits to the metal abundance ($Z/Z_\odot$) in the molecular gas in these galaxies of between 0.9 and 12.9. The main caveat is that we cannot be sure for all galaxies that the CO and C I emission is confined to the region covered by the dynamical analysis.

(v) We have used chemical evolution models to show that it is possible to produce such high metal masses and abundances shortly after the formation of a galaxy as long as the stellar IMF in the galaxy is top-heavy.

(vi) We used these models to show that the metals in the outflows from these galaxies can explain quantitatively the long-standing conundrum that $\simeq$75 per cent of the metals in present-day rich clusters are in the intracluster gas rather than in the galaxies.

(vii) Our estimates of the metal abundance in the DSFGs are sometimes higher than the values of the metal abundance in the galaxies today that are their probable descendants. We speculate that the explanation is the gradual dilution of the metal content by a sequence of dry mergers.

ACKNOWLEDGEMENTS

We thank Tim Davis for comments on an early version of this manuscript. We thank the referee for some useful comments. SE and MS thank the Science and Technology Facilities Council (STFC)

for support (consolidated grant ST/K000926/1). SD acknowledges support from STFC (grant ID: ST/X000982/1)

DATA AVAILABILITY

The ALMA data referenced in Table 2 are in the ALMA archive. All the other observational data are in published papers.

REFERENCES

Aravena M. et al., 2016, MNRAS, 457, 4406
Asplund M., Grevesse N., Sauval A. J., Scott P., 2009, ARA&A, 47, 481
Bakx T. J. L. C. et al., 2018, MNRAS, 473, 1751
Barger A. J., Cowie L. L., Sanders D. B., Fulton E., Taniguchi Y., Sato Y., Kawara K., Okuda H., 1998, Nature, 394, 248
Bisbas T. G., Papadopoulos P. P., Viti S., 2015, ApJ, 803, 37
Bisbas T. G., Tan J. C., Tanaka K. E. I., 2021, MNRAS, 502, 2701
Bolatto A. D., Wolfire M., Leroy A. K., 2013, ARA&A, 51, 207
Boselli A. et al., 2010, PASP, 122, 261
Bothwell M. S. et al., 2017, MNRAS, 466, 2825
Bouché N. F. et al., 2022, A&A, 658, A76
Bovy J., 2022, Dynamics and Astrophysics of Galaxies, https://galaxiesbook.org/index.htm
Cappellari M. et al., 2012, Nature, 484, 485
Clark C. J. R., Schofield S. P., Gomez H. L., Davies J. I., 2016, MNRAS, 459, 1646
Coppin K. E. K. et al., 2010, MNRAS, 407, L103
Cullen F. et al., 2019, MNRAS, 487, 2038
Curti M. et al., 2024, A&A, 684, A75
da Cunha E. et al., 2013, ApJ, 766, 13
Daddi E. et al., 2009, ApJ, 694, 1517
De Breuck C. et al., 2014, A&A, 565, A59
De Breuck C. et al., 2019, A&A, 631, A167
De Vis P. et al., 2017, MNRAS, 464, 4680
De Vis P., Maddox S. J., Gomez H. L., Jones A. P., Dunne L., 2021, MNRAS, 505, 3228
Di Teodoro E. M., Fraternali F., 2015, MNRAS, 451, 3021
Downes D., Solomon P. M., 1998, ApJ, 507, 615
Dunne L., Maddox S. J., Papadopoulos P. P., Ivison R. J., Gomez H. L., 2022, MNRAS, 517, 962
Dye S. et al., 2015, MNRAS, 452, 2258
Dye S. et al., 2022, MNRAS, 510, 3734
Eales S. A., Wynn-Williams C. G., Duncan W. D., 1989, ApJ, 339, 859
Eales S. et al., 2012, ApJ, 761, 168
Eales S., de Vis P., Smith M. W. L., Appah K., Ciesla L., Duffield C., Schofield S., 2017, MNRAS, 465, 3125
Eales S., Lilly S., Gear W., Dunne L., Bond J. R., Hammer F., Le Fèvre O., Crampton D., 1999, ApJ, 515, 518
Fraternali F., Karim A., Magnelli B., Gómez-Guijarro C., Jiménez-Andrade E. F., Posses A. C., 2021, A&A, 647, A194
Fujimoto S. et al., 2023, ApJ, 949, L25
Gallazzi A., Charlot S., Brinchmann J., White S. D. M., Tremonti C. A., 2005, MNRAS, 362, 41
Genzel R. et al., 2017, Nature, 543, 397
Ginolfi M. et al., 2020, A&A, 633, A90
Glover S. C. O., Clark P. C., 2016, MNRAS, 456, 3596
Gong M., Ostriker E. C., Kim C.-G., Kim J.-G., 2020, ApJ, 903, 142
Harrington K. C. et al., 2021, ApJ, 908, 95
Heintz K. E. et al., 2023, Nat. Astron., 7, 1517
Heintz K. E., Watson D., 2020, ApJ, 889, L7
Hodge J. A., Carilli C. L., Walter F., de Blok W. J. G., Riechers D., Daddi E., Lentati L., 2012, ApJ, 760, 11
Hughes D. H. et al., 1998, Nature, 394, 241
Jiménez-Andrade E. F. et al., 2018, A&A, 615, A25
Jones G. C. et al., 2017, ApJ, 850, 180
Jones G. C., Maiolino R., Caselli P., Carniani S., 2019, A&A, 632, L7
Jones G. C., Maiolino R., Circosta C., Scholtz J., Carniani S., Fudamoto Y., 2023, MNRAS, 518, 691
Karakas A. I., Lugaro M., Carlos M., Cseh B., Kamath D., García-Hernández D. A., 2018, MNRAS, 477, 421
Langeroodi D. et al., 2023, ApJ, 957, 39
Lelli F., Di Teodoro E. M., Fraternali F., Man A. W. S., Zhang Z.-Y., De Breuck C., Davis T. A., Maiolino R., 2021, Science, 371, 713
Lilly S. J., Carollo C. M., Pipino A., Renzini A., Peng Y., 2013, ApJ, 772, 119
Lilly S. J., Eales S. A., Gear W. K. P., Hammer F., Le Fèvre O., Crampton D., Bond J. R., Dunne L., 1999, ApJ, 518, 641
Limongi M., Chieffi A., 2018, ApJS, 237, 13
Loewenstein M., 2013, ApJ, 773, 52
Maeder A., 1992, A&A, 264, 105
Maiolino R., Mannucci F., 2019, A&AR, 27, 3
Mernier F., Biffi V., 2022, Chemical Enrichment in Groups and Clusters, in Santangelo A., Bambi C., eds, Handbook of X-ray and Gamma-ray Astrophysics, Springer Nature, p. 4961
Neeleman M., Prochaska J. X., Kanekar N., Rafelski M., 2020, Nature, 581, 269
Nomoto K., Kobayashi C., Tominaga N., 2013, ARA&A, 51, 457
Papadopoulos P. P., Greve T. R., 2004, ApJ, 615, L29
Papadopoulos P. P., van der Werf P. P., Xilouris E. M., Isaak K. G., Gao Y., Mühle S., 2012, MNRAS, 426, 2601
Papadopoulos P., Dunne L., Maddox S., 2022, MNRAS, 510, 725
Peng B. et al., 2023, ApJL, 944, 36,
Peng Y.-j., Maiolino R., 2014, MNRAS, 443, 3643
Planck Collaboration et al., 2016, A&A, 594, A13
Portinari L., Moretti A., Chiosi C., Sommer-Larsen J., 2004, ApJ, 604, 579
Renzini A., Andreon S., 2014, MNRAS, 444, 3581
Reuter C. et al., 2020, ApJ, 902, 78
Rigopoulou D., Pereira-Santaella M., Magdis G. E., Cooray A., Farrah D., Marques-Chaves R., Perez-Fournon I., Riechers D., 2018, MNRAS, 473, 20
Rizzo F., Vegetti S., Fraternali F., Stacey H. R., Powell D., 2021, MNRAS, 507, 3952
Rizzo F., Vegetti S., Powell D., Fraternali F., McKean J. P., Stacey H. R., White S. D. M., 2020, Nature, 584, 201
Roman-Duval J. et al., 2022, ApJ, 928, 90
Romano D., Matteucci F., Zhang Z. Y., Papadopoulos P. P., Ivison R. J., 2017, MNRAS, 470, 401
Rybak M. et al., 2023, A&A, 679, A119
Scholtz J., Maiolino R., Jones G. C., Carniani S., 2023, MNRAS, 519, 5246
Scoville N. et al., 2016, ApJ, 820, 83
Scoville N. et al., 2017, ApJ, 837, 150
Smail I., Ivison R. J., Blain A. W., 1997, ApJ, 490, L5
Spilker J. S. et al., 2016, ApJ, 826, 112
Spilker J. S. et al., 2018, Science, 361, 1016
Tacchella S., Dekel A., Carollo C. M., Ceverino D., DeGraf C., Lapiner S., Mandelker N., Primack J. R., 2016, MNRAS, 458, 242
Tacconi L. J. et al., 2018, ApJ, 853, 179
Tacconi L. J., Genzel R., Sternberg A., 2020, ARA&A, 58, 157
Thomas D., Maraston C., Schawinski K., Sarzi M., Silk J., 2010, MNRAS, 404, 1775
van den Hoek L. B., Groenewegen M. A. T., 1997, A&AS, 123, 305
Veilleux S., Maiolino R., Bolatto A. D., Aalto S., 2020, A&AR, 28, 2
Walter F., Brinks E., Duric N., Klein U., 1997, AJ, 113, 2031
Wardlow J. L. et al., 2017, ApJ, 837, 12
Yin J., Hou J. L., Prantzos N., Boissier S., Chang R. X., Shen S. Y., Zhang B., 2009, A&A, 505, 497
Zhang Z.-Y., Romano D., Ivison R. J., Papadopoulos P. P., Matteucci F., 2018, Nature, 558, 260

APPENDIX A: DIFFERENCES IN THE ISM OF A HIGH-REDSHIFT GALAXY THAT MIGHT LEAD TO A CHANGE IN THE CALIBRATION FACTORS FOR THE ISM TRACERS

We briefly discuss here some of the possible differences between the ISM of a high-redshift galaxy and the ISM of the Galaxy which might lead to a difference in the calibration factor for each of the tracers. We refer the reader to (Dunne et al. 2022) for a fuller discussion. Dunne et al. (2022) made the first attempt to estimate the three calibration factors simultaneously without assuming that one was more reliable than the others. Their sample included 407 galaxies ranging from nearby discs to DSFGs out to $z \simeq 6$.

They estimated the calibration factors by minimizing the variance in the three luminosity ratios: L_{CO}/L_{CI}, L_{CO}/L_{dust}, L_{CI}/L_{dust}. They found no evidence for any variation of these ratios with redshift, in agreement with our conclusion that the ratios of the calibration factors must be the same at high and low redshift. Since there is no way of measuring the mass of molecular gas directly, their method, like those used in all similar studies, was ultimately based on an assumption about the Galactic ISM, in their case that the gas-to-dust ratio is the same as in the Galaxy.

We reproduce here three equations from that paper (equations 9, 10, and 11) which show how the calibration factors depend on the properties of the ISM. We use these equations to discuss how differences between the ISM in a high-redshift galaxy and the Galactic ISM might lead to a change in the calibration factor.

For key equation for C I is:

$$\alpha_{CI} = 16.8 \left[\frac{X_{CI}}{1.6 \times 10^{-5}}\right]^{-1} \left(\frac{Q_{10}}{0.48}\right)^{-1} M_{\odot}(\mathrm{K\ km\ s^{-1}\ pc^2})^{-1} \quad \text{(A1)}$$

in which $X_{CI} = [C^0/H_2]$, the abundance ratio of carbon atoms relative to hydrogen molecules, and Q_{10} is the is fraction of the carbon atoms in the J = 1 state.

The calibration factor might be different from the value assumed in this paper if either X_{CI} or Q_{10} are different from the values assumed by Dunne et al. (2022). The dependence of Q_{10} on the density and temperature of the gas in none-LTE conditions is derived analytically in the appendix of Papadopoulos & Greve (2004). Figure D1 in Appendix D of Dunne et al. (2022) shows that for a reasonable range of n ($300 < n < 10,000$ cm^{-3} and T_K ($25 < T_k < 80$ K) Q_{10} does not go outside the range 0.35 to 0.53. Therefore, it seems unlikely that changes in the density and temperature of the gas will lead to large changes in the calibration factor. In particular, changing the value from that assumed by Dunne et al. (2022) (0.48) to 0.53 will only lower the calibration factor by a factor of $\simeq$10 per cent.

The other factor, X_{CI} depends in a straightforward way on the metal abundance and the fraction of carbon that is the atomic form. The first of these we don't discuss here because this is our alternative explanation of the change in the calibration factor. A plausible reason why the proportion of atomic carbon might be higher in a high-redshift DSFG, which would lead to a lower value of α_{CI}, is that the density of cosmic rays might well be higher, which would lead to a change in the carbon chemistry and increase the abundance of C I relative to CO (Bisbas et al. 2015; Glover & Clark 2016; Gong et al. 2020; Bisbas et al. 2021; Dunne et al. 2022). We note, though, that Dunne et al. (2022) do not find any difference between the value of α_{CI} for high-redshift DSFGs and galaxies at the same redshift with lower star-formation rates, which would be likely to have lower densities of cosmic rays.

The key equation for dust is:

$$\alpha_{850} = \frac{1.628 \times 10^{16}}{1.36\kappa_H} \left(\frac{24.5}{T_{mw}}\right)^{-1.4} \mathrm{W\ Hz^{-1}\ M_{mol}^{-1}} \quad \text{(A2)}$$

in which T_{mw} is the mass-weighted dust temperature and κ_H is a constant of proportionality linking the mass of gas and the mass of dust. The latter depends in a straightforward way on the metal abundance, the fraction of the metals in the dust grains, and the submillimetre mass-opacity coefficient (the submillimetre opacity for a unit mass of dust).

The explanation of a difference in the calibration factor is unlikely to be a difference in T_{mw} because the values we directly estimated for six of our sample (Table 3) are similar to the value assumed in Dunne et al. (2022) (24.5 K). We don't discuss a change in the metal abundance here because this is our preferred explanation of the change in the calibration factor. The fraction of the metals bound up in dust grains is already high in the Galaxy (0.52, Roman-Duval et al. (2022), so it seems unlikely it would be much higher in a high-redshift DSFG.

The most plausible way to change this calibration factor would be if the dust grains in the DSFG are different in some way – in their chemistry, structures, shapes or sizes – from those in the Galaxy (Clark et al. 2016). The easiest way to make the calibration factor smaller would be if the dust grains are smaller than in the Galaxy, increasing the total surface of the dust grains for a given mass of dust.

On the large-velocity-gradient assumption, the key equation for CO is:

$$\alpha_{CO} = 2.65 \frac{\sqrt{n_{H_2}}}{T_b} K_{vir}^{-1} [M_{\odot} \mathrm{K\ km\ s^{-1}\ pc^2}]^{-1} \quad \text{(A3)}$$

in which n_{H_2} in the average density of the molecular gas in cm^{-3}, T_b is the brightness temperature of the CO 1–0 line and K_{vir} describes the average dynamic state of the gas (Dunne et al. 2022). The obvious way to make this calibration factor smaller in the DSFG if is if the density of the gas is lower and/or the temperature is higher, which is plausible since the intensity of the optical/UV radiation field is likely to be higher in a high-redshift DSFG because of its higher star-formation rate. We note, though, that Dunne et al. (2022) do not find any difference between the value of α_{CO} for high-redshift DSFGs and galaxies at the same redshift with lower star-formation rates. We also note that two of the key results of the most extensive multi-line CO observations of high-redshift DSFGs (Harrington et al. 2021) are (a) that the ISM in these galaxies is dominated by warm dense gas and (b) that the calibration factor is similar to its Galactic value.

APPENDIX B: CORRECTION FOR THE EFFECT OF ASYMMETRIC DRIFT

We have made a correction to the dynamical masses for the effect of stellar pressure (asymmetric drift) for the six galaxies for which this correction was not made in the original analysis in the literature, using the formalism given in appendix A of Bouché et al. (2022). The gravitational potential is given by:

$$\frac{GM(<r)}{r} = v_{rot}^2 + \eta\sigma^2 \left(\frac{r}{r_d}\right) \quad \text{(B1)}$$

in which v_{rot} is the rotational velocity, σ is the velocity dispersion, r_d is the scale length of the disc, and η is a numerical constant of order unity. The value of η depends on the model assumed for the disc (Bouché et al. 2022). We have assumed a value of 1 appropriate

for a disc in which the disc thickness and velocity dispersion have no radial dependence. The fractional correction to the masses for asymmetric drift is given by the ratio of the second to the first term on the right-hand side of the equation. We have estimated this from the data in the original papers, and our estimates are listed in Table 4. For all but two galaxies the correction is ≤ 10 per cent. We have used these estimates to correct the masses for asymmetric drift for the seven galaxies in the sample for which this effect was not included in the original analysis.

This paper has been typeset from a TEX/LATEX file prepared by the author.